periodica polytechnica

Mechanical Engineering
53/2 (2009) 75–80
doi: 10.3311/pp.me.2009-2.04
web: http://www.pp.bme.hu/me

RESEARCH ARTICLE

Formation of surface layer on cast iron cylinder bore due to nanosecond laser impulses

Kornél Májlinger / *Péter J.* Szabó / *Kristóf* Bobor

Received 2010-01-18

Abstract

The air pollution emission standards for automobiles are going to be more strict worldwide. European automotive manufacturer makes a laser treatment on the cast iron cylinder bores of the V-engine blocks. Samples of laser treated cast iron cylinder bore with lamellar graphite were investigated. Seven samples were treated with XeCl-excimerlaser, Nd-YAG laser and Yb-fiber laser sources. In order to evaluate the microstructure and grain size of the laser treated layer, scanning electron microscopic (SEM) images were taken in cross section with a SEM/focused ion beam (FIB) dual beam electron microscopes. All the samples were found to be ultra fine grained. To simulate the heating conditions during laser treatment, finite element method (FEM) simulations were made for the different lasertypes. Additional X-ray diffraction measurements showed retained austenite after laser treatment.

Keywords

laser treatment · cast iron · cylinder bore · FEM simulation · FIB

Acknowledgement

The authors want to thank the II. Institute of Physics of the University of Göttingen, and the Hungarian Research Institute for Technical Physics and Materials Science (MFA), where the focused ion beam investigations were made. Additionally thanks to Dr. Ádám Révész for the XRD measurements.

Kornél Májlinger
Department of Materials Science and Engineering, BME, H-1111 Budapest, Bertalan Lajos u. 7., Hungary
e-mail: pmgpwo@hotmail.com

Péter J. Szabó
Department of Materials Science and Engineering, BME, H-1111 Budapest, Bertalan Lajos u. 7., Hungary
e-mail: szpj@eik.bme.hu

Kristóf Bobor
Department of Materials Science and Engineering, BME, H-1111 Budapest, Bertalan Lajos u. 7., Hungary
e-mail: hoacin@freestart.hu

1 Introduction

The automotive engine development is defined by three main factors: (I) to make the engines more cost effective, (II) to keep the environmental regulations and (III) the increasing fuel prices, which means that by even higher engine power the fuel and oil consumption should not increase, and the engines should have a long lifetime [1]. Both the consumption reduction and the power increase of Otto- or Diesel-engines cause higher pressures in the combustion chamber resulting higher tribological load and wear rate for the piston rings and to the cylinder bore [1].

To improve mechanical and tribological properties of cast iron cylinder bores it is possible to use special mechanical [2] and laser structuring treatments [3], or – which is used by a large European automotive manufacturer – a special laser treatment on the V-block engines to alter the properties of the cylinder bores. Due to the laser treatment, the near surface area of the cylinder bore becomes harder and more wear resistant, furthermore, due to the inhomogenity of the pearlitic matrix and carbon lamellae, oil reserving holes are formed. This treatment results in an increased power output and reduced oil consumption [1, 4].

2 The laser treatment

The goal of the laser treatment is to melt a thin layer on the surface and at the same time the laser induced plasma over the surface evaporates the graphite lamellae, deeper than the metallic surface itself. So these "holes" are practically non-communicating oil reservoirs [1]. This treatment is patented, the patent number is EP 1 738 859 A1.

Recently the cylinder bores in the mass-production are treated with a Xe-Cl excimer laser which works in the UV wavelength region (308 nm). During treatment the workpiece is lasered with a rectangular laserspot with 4 times overlap in a definite raster. The adjustable parameters during the laser treatment are: (I) scale of the overlap (scanning grid), (II) mean laser energy density on the surface and (III) the speed of the scanning.

There are further experiments to find alternative laser sources, because the excimer lasers have high maintenance requirements and the maintenance and servicing costs are higher than those

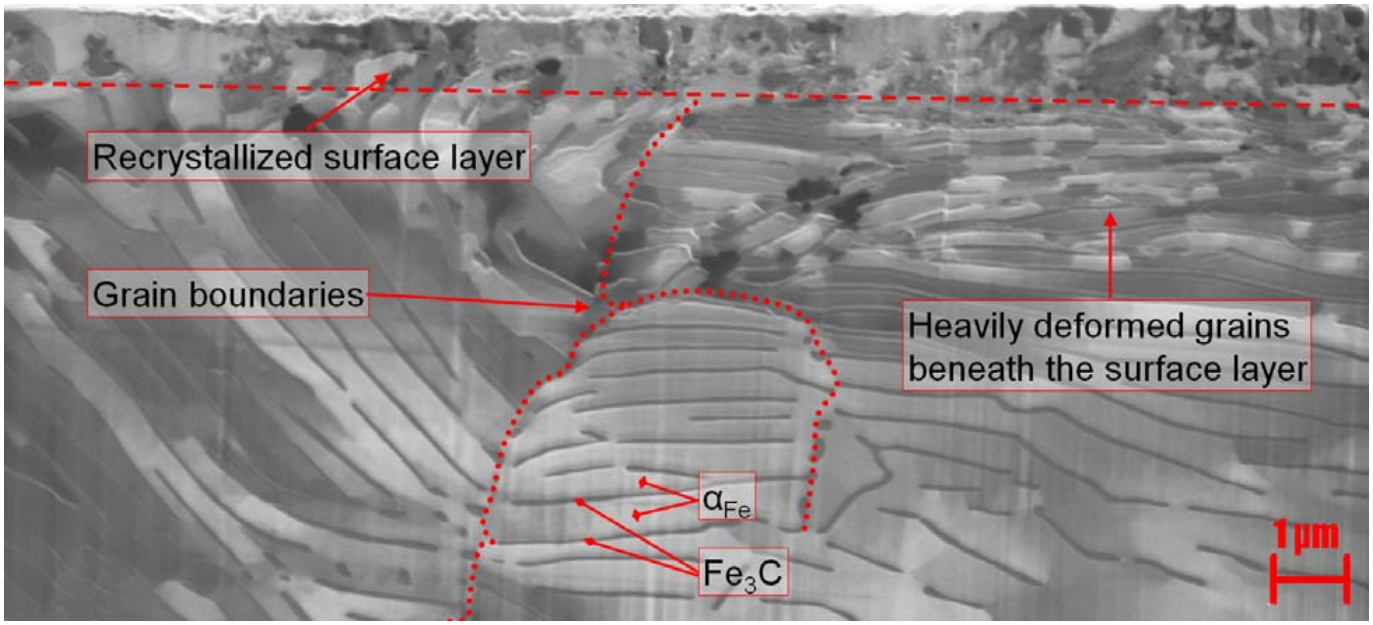

Fig. 1. Ga-ion image of the wall of a cavity made by ion-beam from sample "A"

of the solid states lasers. A further disadvantage of the currently applied excimer laser is that because of the geometry of the optical output system during laser treatment, the whole cylinder block has to be rotated around the laser output window which significantly reduces the efficiency of the laser system. Furthermore, excimer lasers have large space requirements too.

We investigated seven samples, treated with Nd-YAG laser and Yb-fiber laser sources in three different configurations. The material of the samples is grey cast iron with lamellar graphite (GJL-250). The main laser parameters for the laser treatment are shown in Table 1.

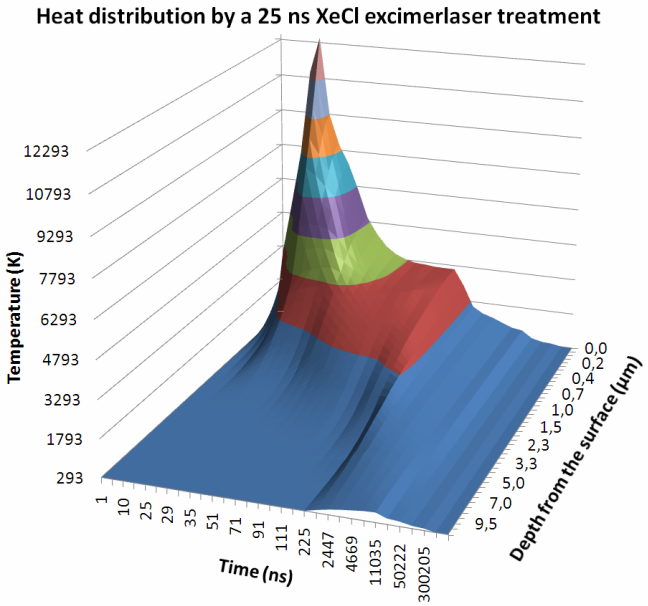

Fig. 2. Temperature distribution (FEM) during and after laser treatment by a 25 ns laser impulse in sample "A"

3 Experimental

Finite element simulations. The thermal processes during the laser treatment were simulated through finite element method. For these simulations 8-node 2D quadratic elements were used.

During the calculations the following simplifications were applied. The power output of the laser changed like a step function, i.e. at the beginning and at the end of the impulse it was changing quickly and during the impulse was constant. The energy density distribution within the laser spot was considered uniform. The surface was analyzed in a point far enough from the laser-spots edge and so the heat flow parallel to the surface could be neglected. The material was considered homogeneous. The latent heat by allotrope transition was neglected (by melting and boiling it was taken into account), and the material properties over the melting point (specific heat and thermal conductivity) were taken as constants. The evaporation of the very top surface layers by the laser ablation were not taken into account. As a boundary condition, a fixed temperature point (environment temperature, 293 K) was set far enough from the surface.

Focused Ion Beam investigation. The focused ion beam investigations were made by a FEI Nova Nanolab 600 SEM/FIB dual beam and with a LEO Gemini cross beam SEM/FIB scanning electron microscope. Both are combination of a scanning electron microscope and a Ga-ion beam source, and so are capable to machine structures less than 100 nm size and are usable for prototyping and analysis. It combines the very high resolution of the electron microscope with field emission cathode and the etching, ion deposition and ion evaporation abilities of a focused ion beam source. With this equipment it is possible to image the surface of the specimen either with the electron or with the ion beam [5, 6]. During imaging half of a regular cross section for TEM lamellae cutout were made with the ion beam and then images were taken – with lowered ion current –

Tab. 1. Main laser parameters for laser treatment

Sample	Laser type	Wavelength	Pulse duration	Repetition frequency	Energy density on the surface
A	Xe-Cl Excimer	308 nm	25 ns	300 Hz	27.5 mJ/mm^2
B	Nd-YAG	1064 nm	40 ns	6000 Hz	52.0 mJ/mm^2
C	Nd-YAG	1064 nm	165 ns	6000 Hz	55.6 mJ/mm^2
D	Yb-Fiber	1065 nm	140 ns	12500 Hz	26.7 mJ/mm^2
E	Yb-Fiber	1065 nm	140 ns	12500 Hz	31.6 mJ/mm^2
F	Yb-Fiber	1065 nm	140 ns	12500 Hz	37.0 mJ/mm^2
G	Yb-Fiber	1065 nm	140 ns	12500 Hz	42.0 mJ/mm^2

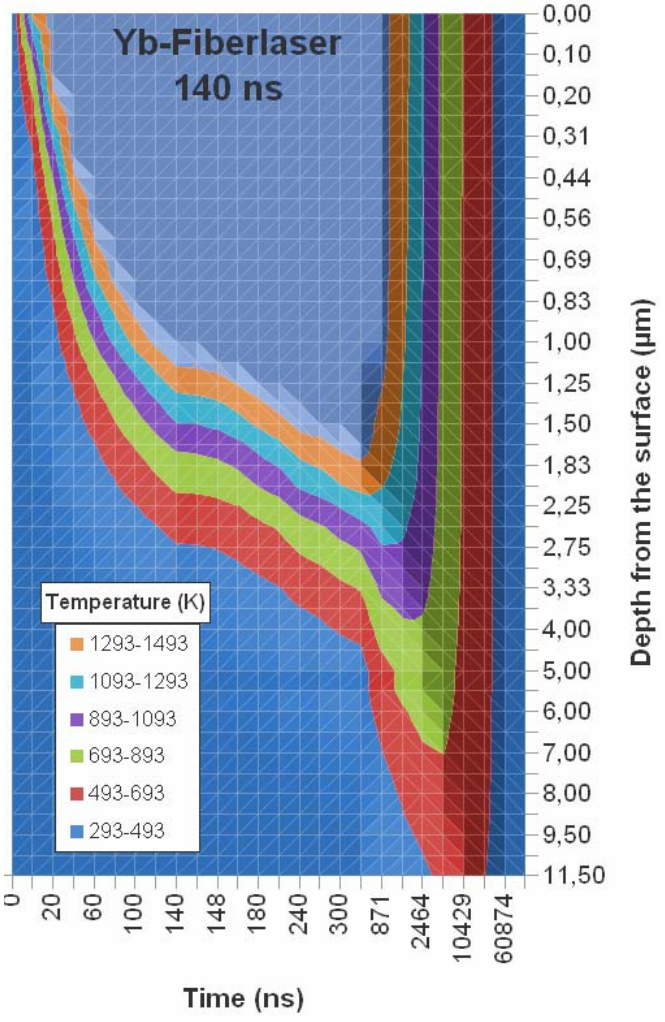

Fig. 3. Temperature profile (FEM) of the Yb-fiberlaser treated sample "D"

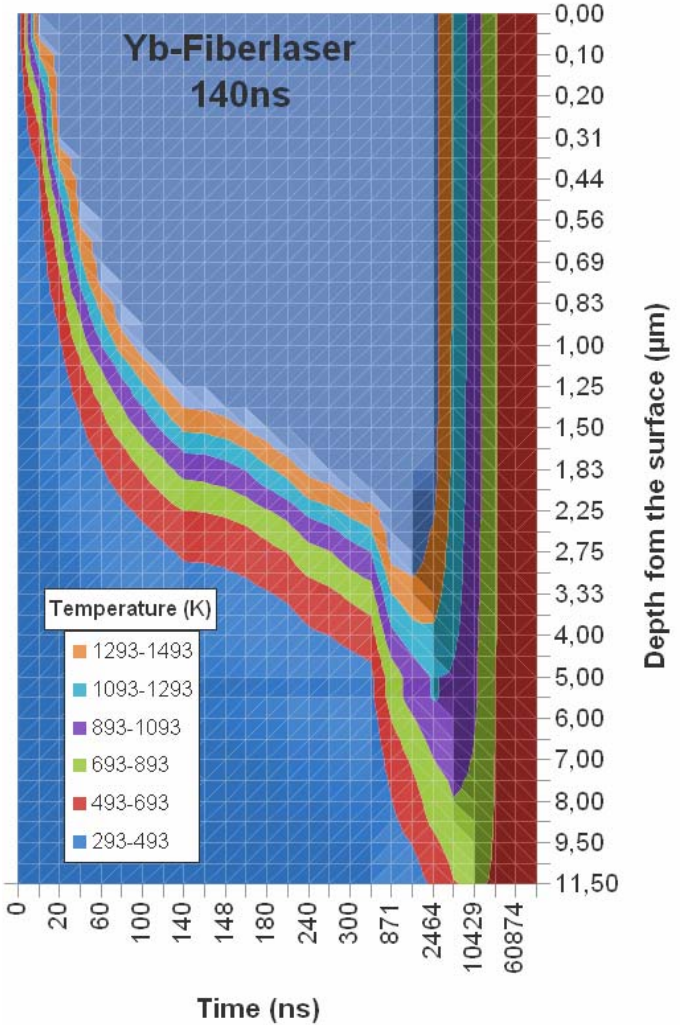

Fig. 4. Temperature profile (FEM) of the Yb-fiberlaser treated sample "G"

of the wall of the obtained cavity (Fig. 1) [7]. To determine the average grain size and layer thickness several FIB images were merged together with Corel Draw software, to cover an area of approx. 20 ×7μm (20 μm in horizontal and 7 μm in vertical direction). The average grain size was determined along 3 lines (3 horizontal lines were drawn into the laser treated layer – from grain boundary to grain boundary – and the number of the grains along these lines with known length were counted).

Further SEM investigations were made with a Philips XL 30 electron microscope on samples prepared like standard metallographic samples.

X-ray diffraction (XRD). XRD measurements were made on the laser treated surface of the samples. The XRD investigations were made with a Philips X'Pert Diffractometer CoKα source with Fuji Imaging Plates (BAS-MS 2025) with a spotsize of 100x500 μm^2.

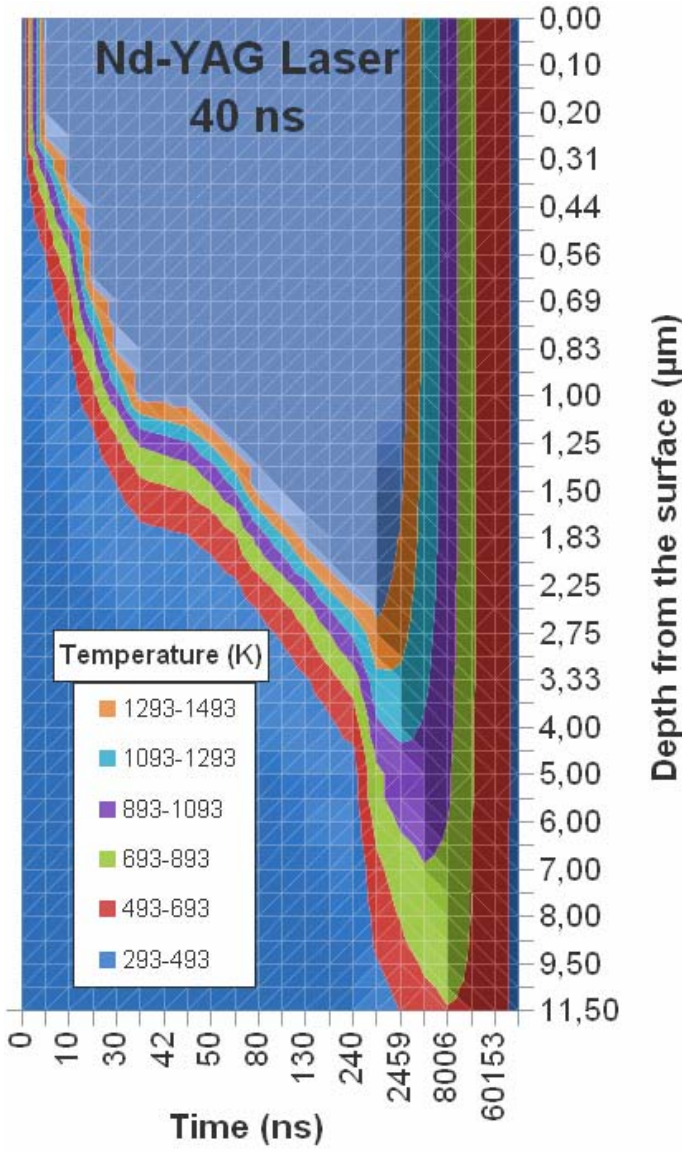

Fig. 5. Temperature profile (FEM) of the Nd-YAG laser treated sample "B"

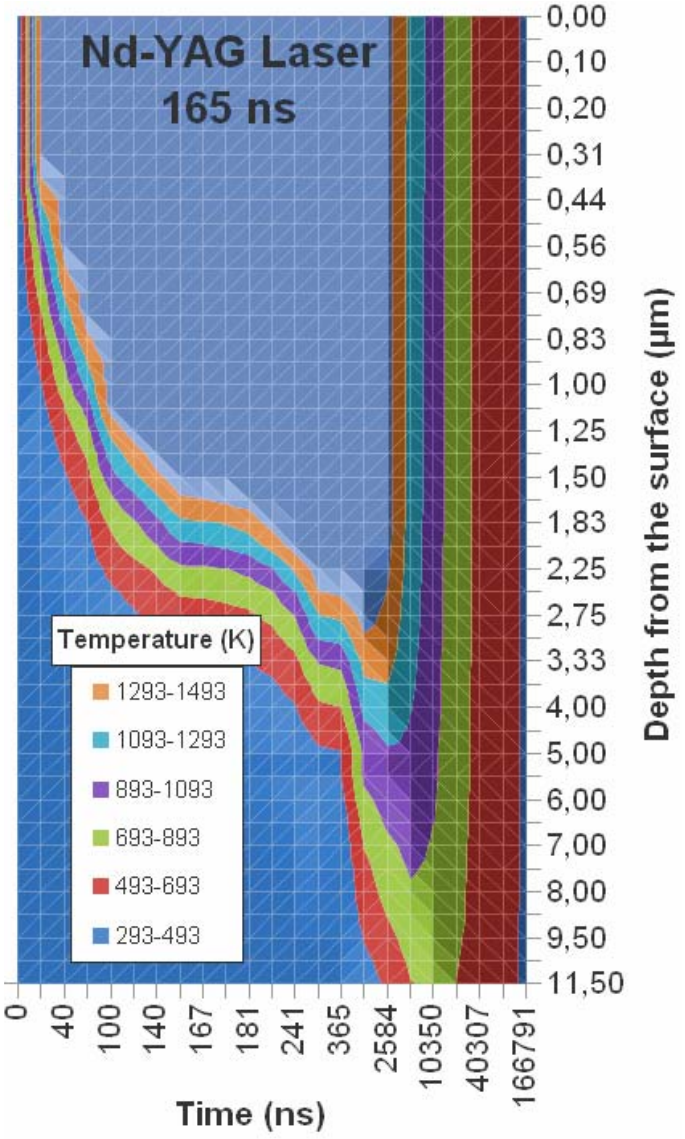

Fig. 6. Temperature profile (FEM) of the Nd-YAG laser treated sample "C"

4 Results and discussion

Finite element simulations. The temperature distribution obtained by the FEM simulations were displayed in 3D diagrams like Fig. 2. The calculated melting depths are displayed in Table 2. The calculated depth above the austenising temperature is also displayed in Table 2.

As expected the calculated austenising depth and the calculated depth of the molten layer is growing with increasing laser energy densities (Fig. 3 – Fig. 6).

The simulation suggests that altough the depth of the molten layer is dependent by the laser energy density mostly (Fig. 3 – Fig. 4), the austenitised depth is also strongly dependent by the duration of the laser pulse (Fig. 5 – Fig. 6). The longer the laser pulse duration the deeper the expected austenising. The calculated melting depths are close to the measured values but quantitatively they are a bit higher because in the model very many simplifications were made.

The calculated temperature profile of the topmost surface layer for the different laser energy densities and laser pulse durations is displayed in Fig. 7. It is clearly seen in Fig. 7 that the shorter laser pulse results in a higher surface temperature and narrower heat gradient, because the energy density per nanosecond is higher. The cooling time back to the boiling temperature seems to be only dependent by the laser energy density.

The model is overall a good tool to qualitative simulation to compare different lasertypes with different laserpulse duration and maybe to adjust an existing manufacturing system.

The temperature profiles are comparable to other more refined simulations – made by finite difference method by Schaaf [8] – in this energy density regime for iron.

Focused ion beam investigations. On the FIB cross section images (Fig. 1) it is well seen that the laser treated layer of the pearlitic cast iron is fine grained. The average grain sizes were between 150 nm and 330 nm so the top layer can be considered ultra fine grained. Below this layer the base material has many larger grains. The grains of the base material are slightly curved in one direction due to the mechanical machining (milling, bore and honing) of the cylinder bores.

Tab. 2. The simulated austenizations (A_{FEM}) and molten layer (R_{FEM}) depths and the measured thickness (R) and grain size (d) of the laser treated layer of the cylinder bores obtained from FIB and SEM images

Sample	A_{FEM} (μm)	Thickness of the laser treated layer			d_{FIB} (nm)
		R_{FEM} (μm)	R_{FIB} (μm)	R_{SEM} (μm)	
A	2.47	1.70	0.96 – 1.23	0.92 – 1.54	325
B	5.30	2.39	0.65 – 0.71	0.57 – 1.01	179
C	6.15	2.76	0.85 – 1.18	0.65 – 1.19	222
D	3.28	1.70	0.90 – 1.04	0.32 – 1.35	243
E	4.92	2.26	0.41 – 0.91	0.55 – 2.07	148
F	5.84	2.63	0.73 – 0.97	0.56 – 1.57	215
G	6.14	2.79	0.93 – 1.13	0.76 – 2.11	204

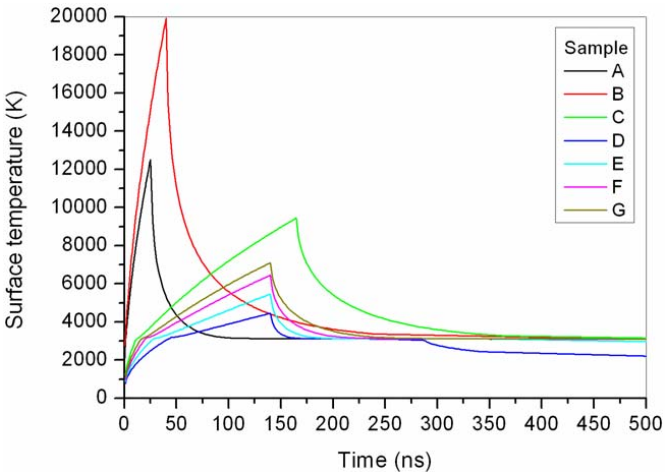

Fig. 7. Temperature of the surface (FEM) by different laser pulse duration and energy densities

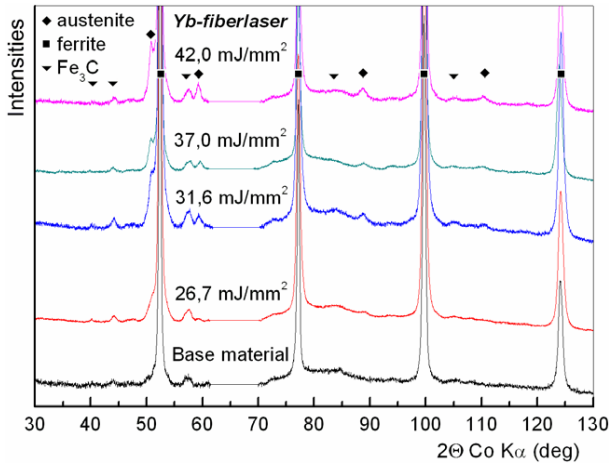

Fig. 8. X-ray diffraction patterns of the Yb-fiberlaser treated samples and of an untreated sample

The ultra-fine grained structure was most formed because of the large heat gradient during solidification of the molten surface.

The measured layer thicknesses of the molten surface are given in Table 2, the values were between 0.5 μm - 2 μm depending on the measurement type (FIB/SEM) and place on the sample. Because of the mechanical deformation due to the machining (drilling and 3 step hone process) prior to the laser treatment and because of the heterogenous microstructure of the base material the range of the measured layer thicknesses is broad. To determine the molten layer thickness more precise, further laser treatment probes on flat surface should be made.

XRD investigation. The XRD measurements showed that a new phase was formed after laser treatment. The phase was identified as austenite. The x-ray diffraction patterns of the Yb-laser treated samples and an untreated sample is shown in Fig. 8. It is clear that the proportion of the new phase is growing with increasing laser energy density, which is in good accordance with the FEM simulations of increasing austenisations depth. Retained austenite was present in every laser treated sample by all laser types and laser energies, as it has been reported in many other cases and for different laser types [8]-[12] too.

5 Conclusions

The top layers of the laser treated cylinder bores were molten and at the place of outburned graphite holes non-communicative oil reserving holes were formed. The FEM simulations showed comparable layer thickness to the measured FIB and SEM layer thicknesses. The recrystallised surface layers were found to be ultra fine grained. Retained austenite – which proportion is growing with the higher energy densities and longer laser pulse durations – was found in all the laser treated samples. It is not cleared yet if the retained austenite is transformed into martensite in the surface and near surface area.

References

1 **Lindner H, Bergmann H. W, Brandenstein C, Lang R, Queitsch A, Reichstein S, Stengel E**, *UV-Laserbelichtung von Grauguß-Zylinderlaufbahnen von Verbrennungskraftmaschienen*, VDI-Berichte (2003), no. 1764, 73-96.

2 **Knoll G, Lagemann V, Lechtape-Grüter R, Robota A, Schlerege F**, *Beeinflussung des Ölverbrauchs von Verbrennungskraftmaschienen durch die Mikrohydrodynamik strukturierter Zylinderoberflächen*, VDI-Berichte (2003), no. 1764, 63-72.

3 **Andersson P, Koskinen J, Varjus S, Gerbig Y, Haefke H, Georgiou S, Zhmudd B, Buss W**, *Microlubrication effect by laser-textured steel surfaces*, Wear **262** (2007), 369–379.

4 **Herbst L, Lindner H, Heglin M, Hoult T**, *Targeting diesel engine efficiency, Industrial Laser Solutions for manufacturing*, 2004, available

at www.coherent.com/Downloads/dieselengine_ilsRev2.pdf. Application report.

5 2008.04.10, available at http://www.nanoscience.hu/education/anyagtudomany/08_pasztazo.pdf.

6 2008. 05.18., available at http://www.fei.com/uploadedFiles/Documents/Content/2006_06_Nova600NanoLab_pb.pdf.

7 **Májlinger K, Szabó P. J**, *Measuring the Effects of Some Laser Parameters on the Surface and Near Surface Region of Laser Treated Cast Iron Cylinder Bore*, Per. Pol. Mech. Eng. **52** (2008), no. 2, 71-76, DOI 10.3311/pp.me.2008-2.06.

8 **Schaaf P**, *Laser nitriding of metals*, Progress in Material Science **47** (2002), no. 1, 1-161.

9 **Benyounis K Y, Fakron O M A, Abboud J H, Olabi A G, Hashmi M J S**, *Surface melting of nodular cast iron by Nd-YAG laser and TIG*, Journal of Materials Processing Technology **170** (2005), 127-132, DOI 10.1016/j.jmatprotec.2005.04.108.

10 **Alabeedi K F, Abbouda J H, Benyounisb K Y**, *Microstructure and erosion resistance enhancement of nodular cast iron by laser melting*, Wear **266** (2009), 925-933, DOI 10.1016/j.wear.2008.12.015.

11 **Lian S, Chenglao L**, *Effect of laser melting processing on the microstructure and wear resistance of gray cast iron*, Wear **147** (1991), 195-206, DOI 10.1016/0043-1648(91)90129-I.

12 **Benkißer G, Pohl M, Heßing C**, *Effects of Laser Remelting on the Microstructure and Hardness of Grey Cast Iron Containing Lamellar ad Globular Graphites*, Prakt. Metallogr. **43** (2006), 381-395.